communications physics

ARTICLE

https://doi.org/10.1038/s42005-023-01251-8 OPEN

Flux-flow instability across Berezinskii Kosterlitz Thouless phase transition in $KTaO_3$ (111) based superconductor

Shashank Kumar Ojha [1,2]✉, Prithwijit Mandal [1,2], Siddharth Kumar [1], Jyotirmay Maity[1] & Srimanta Middey [1]✉

The nature of energy dissipation in 2D superconductors under perpendicular magnetic field at small current excitations has been extensively studied over the past two decades. However, dissipation mechanisms at high current drives remain largely unexplored. Here we report on the distinct behavior of energy dissipation in the $AlO_x/KTaO_3$ (111) system hosting 2D superconductivity in the intermediate disorder regime. The results show that below the Berezinskii Kosterlitz Thouless (BKT) phase transition temperature (T_{BKT}), hot-spots and Larkin Ovchinnikov type flux-flow instability (FFI) are the major channels of dissipation, leading to pronounced voltage instability at large currents. Furthermore, such FFI leads to a rare observation of clockwise hysteresis in current-voltage characteristics within the temperature range $T_{BKT} < T < T_C$ (T_C is superconducting transition temperature). These findings deepen our understanding of how a BKT system ultimately transforms to a normal state under increasing current.

[1] Department of Physics, Indian Institute of Science, Bengaluru 560012, India. [2] These authors contributed equally: Shashank Kumar Ojha, Prithwijit Mandal. ✉email: shashank@iisc.ac.in; smiddey@iisc.ac.in

The ability to conduct dissipationless electrical current is one of the most striking features of a superconductor[1]. The phenomena of pair breaking puts an upper theoretical bound on the maximum current that a superconductor can withstand without dissipation[2]. However, a finite dissipation always sets in at much lower current densities in reality, leading to breakdown of the superconductivity (SC) much before the pair breaking limit is reached. Therefore understanding dissipation mechanism is not only critical to answering some of the fundamental questions about the nature and origin of superconductivity, but will also be pivotal in realizing next generation applications such as superconducting digital memory, cavities for particle accelerators and THz radiation sources etc.[3–6].

In 1D, phase slip centers are the primary cause of dissipation[1]. In 2D, an additional complication arises due to occurrence of a topological phase transition which belongs to the Berezinskii Kosterlitz Thouless (BKT) universality class[7,8]. Below the BKT phase transition temperature (T_{BKT}), bound vortex-antivortex pairs are the bare topological excitations which become unbound above the T_{BKT}[8–11]. Nonetheless, some bound vortex-antivortex pairs still exist even in the temperature range $T_{BKT} \leq T \leq T_C$ under zero electrical current (I)[12]. Application of I leads to a further increase in free vortex density due to unbinding of bound vortex-antivortex pairs. These free vortices feel magnus force under the applied current and hence can move with very high velocities at large currents[3]. While the presence of ultra-fast moving vortices and its possible connection with phase slip lines (which are 2D analog of phase slip centers) has been demonstrated earlier[13–17], what happens to these topological defects just before the breakdown remains puzzling. One of the proposition has been that such fast moving vortices can become unstable at large currents leading to flux-flow instability (FFI) as proposed by Larkin and Ovchinnikov (LO)[18,19]. While such a scenario has been demonstrated under magnetic field[3,19–27], its manifestation in BKT systems in absence of external magnetic field remains scarce[28].

The presence of disorder in samples, which is inevitable in reality, further complicates this problem by turning the BKT system inhomogeneous. Such inhomogeneities might range from atomic level point defects to macroscopically phase separated regions[29–32]. While the former determines the vortex pinning strength, the latter often leads to a network of superconducting puddles joined by weak superconducting links. Such weak links, which are hosts of hot-spots, are very fragile under large electric field and are another competing source of dissipation under large current in the absence of magnetic field[33]. In the past, much of the attention has been paid to understanding the dissipation in either very clean or dirty system. Notably, all of these measurements have been primarily performed in the presence of magnetic field (under very small I) and very little is known about the nature of dissipation under large current[16,28,34]. Further, what happens in the intermediate disordered regime also remains an open question.

In recent years, oxide heterostructure based interfacial superconductors have turned out to a potential platform for understanding SC in 2D limit and the focus has been primarily on $SrTiO_3$ (STO) based systems[35–38]. Recently, SC has been discovered at the interface and surface of (111) oriented $KTaO_3$ (KTO) (see Fig. 1a) with $T_C \sim 1.5$–2.2 K[39–42]. The T_C is one order of magnitude higher than heavily investigated STO based heterostructure[35,43] and hence has generated tremendous excitement in the field of interfacial SC. Interestingly, SC was also found to be strongly influenced by the choice of over-layer grown on KTO (111) substrate. For example, the presence of a magnetic element in the overlayer could lead to a stripe order near superconducting transition[39]. While the current focus is on understanding the origin of higher T_C[44] and possible role of spin-orbit coupling (SOC), the nature of dissipation at large current drive remains completely unknown in KTO based systems. Surprisingly, this issue also remains unexplored for any oxide based interfacial superconductors.

In this work, we investigate the underlying mechanisms that cause dissipation at high current drives in KTO (111) based interfacial superconductor. Through a combination of thorough transport measurements and analysis, we have identified strong indications of LO type FFI in association with Joule heating effects. While such a behavior had previously been observed in type II superconductors under the influence of a magnetic field[3,19–27], experimental evidence of such instabilities in the absence of an external magnetic field has remained elusive until now.

Results

Two-dimensional superconductivity in $AlO_x/KTaO_3$ (111) with intermediate disorder. In order to avoid the potential complications caused by a magnetic overlayer on the nature of dissipation, we have fabricated a new superconducting interface by ablating non-magnetic Al_2O_3 on KTO (111) substrate [dimension 5 mm × 5 mm × 0.5 mm] by pulsed laser deposition technique (see Methods, Supplementary Note 1 and Supplementary Fig. 1). The resultant film is amorphous. For electrical transport measurements, two Hall bars were patterned along two in-equivalent crystallographic directions: $[11\bar{2}]$ and $[1\bar{1}0]$ (Fig. 1b) by selective scratching of film deep into the substrate[45]. Figure 1c shows the sheet resistance (R_S) vs. temperature plot of a 7 nm AlO_x/KTO (111) sample. As evident, the interface exhibits metallic behavior down to low temperature confirming the formation of two dimensional electron gas (2DEG). The origin of the 2DEG is connected to the creation of oxygen vacancies (OVs)[42,46] within the top few layers of the KTO substrate. Further, a clear superconducting transition is observed with negligible anisotropy e.g. $T_C = 1.55$ K and 1.51 K for current driven along $[11\bar{2}]$ and $[1\bar{1}0]$, respectively (inset of Fig. 1c) (T_C is estimated from the condition $R_S(T_C) = 0.5 \times R_S(5\text{ K})$). While the value of T_C is very similar to the previous reports[39,40], the observation of little anisotropy is in sharp contrast with the report of large in-plane anisotropy for EuO/KTO (111) near the superconducting transition, T_C[39].

Before discussing the nature of dissipation, we first investigate the nature of this new superconducting system in terms of its dimensionality and the extent of the disorder. To study this, temperature-dependent measurements of R_S (T) under perpendicular ($B_\perp$) and parallel ($B_\parallel$) magnetic fields have been carried out. Figure 1d shows one representative set of data for current along $[11\bar{2}]$ under low $B_\perp$ (for other current orientation see Supplementary Fig. 3). Clearly, the SC is disrupted at very low magnetic field, which can be attributed to the low pinning of vortices in 2D superconductors. Upon increasing the field, the sample avoids superconductor to insulator transition around $R_S \sim 1\ \text{k}\Omega\text{sq.}^{-1}$ as seen in Fig. 1e. This result is in sharp contrast to the conventional theoretical framework that predicts a direct transition to an insulating state when the normal state sheet resistance approaches the quantum of resistance $h/4e^2 = 6.45\ \text{k}\Omega\ \text{sq.}^{-1}$ in the limit $T \to 0$[47,48]. Such a behavior is generally observed in 2D superconductors with low disorder and has proven critically important for studying phases beyond the Landau Fermi liquid theory[49]. Interestingly, at higher $B_\perp$ and lower T, our sample exhibits a logarithmic dependence of R_S on T. This logarithmic divergence is incompatible with the prediction of weak localization correction in 2D or Kondo effect[49] and is connected with the emergent granular nature of our conducting interface[50,51].

To verify that superconductivity is indeed 2D in nature, out of plane and in plane upper critical fields ($B_{C_\perp}$ and $B_{C_\parallel}$) have been measured. Figure 2a shows the temperature dependence of $B_{C_\perp}$

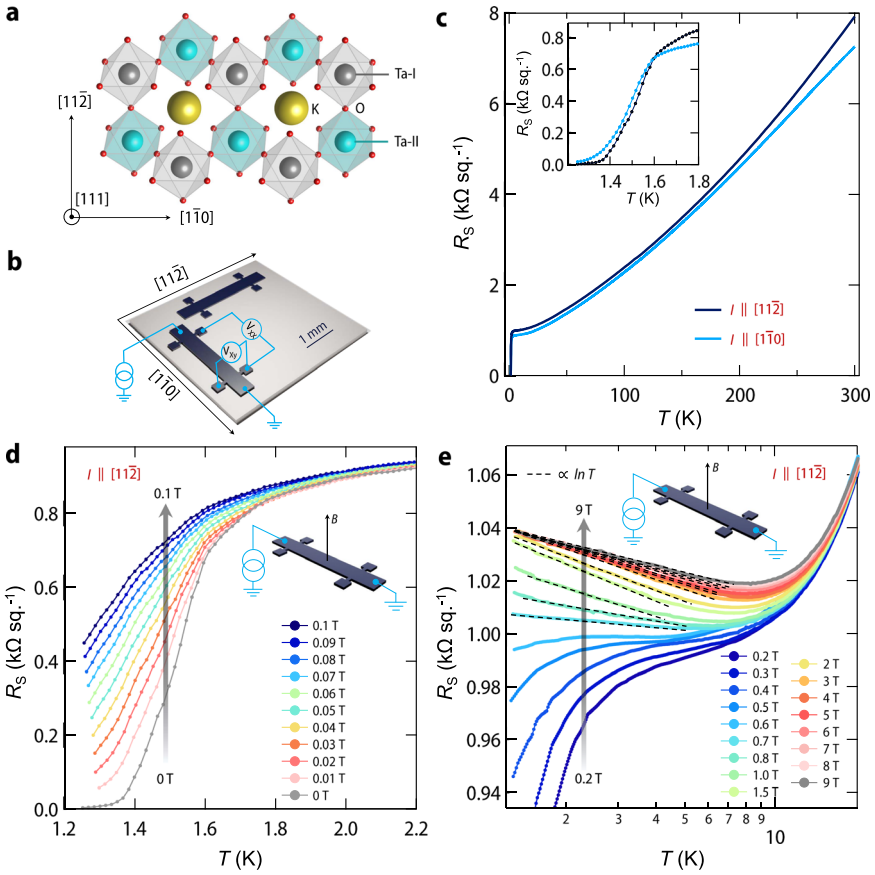

Fig. 1 Device geometry and transport behavior of $AlO_x/KTaO_3$ (111) interface. a In a pure ionic picture, (111) oriented $KTaO_3$ can be considered as a sequence of alternating $[KO_3]^{5-}$ and Ta^{5+} planes. Arrangement of Ta^{+5} ions in two adjacent (111) planes are labeled by Ta-I and Ta-II[69]. **b** Schematics of two Hall bars made on a $AlO_x/KTaO_3$ (111) heterostructure. The width of the Hall bar is 476 μm and 445 μm for [11$\bar{2}$] and [1$\bar{1}$0] directions, respectively and the length between the voltage probes is 1.87 mm for both the Hall bars. **c** Temperature-dependent R_S for both the Hall bars for a 7 nm $AlO_x/KTaO_3$ (111) sample. Inset shows a magnified view around the superconducting transition temperature. The normal state R_S (T) shows a non Fermi liquid behavior ($R_S \propto T^{\alpha}$ where $\alpha < 2$) in a broad range of temperatures from 75 K to 300 K with $\alpha = 1.5$ and 1.3 for current along [11$\bar{2}$] and [1$\bar{1}$0], respectively. This behavior is in sharp contrast with the T^3 behavior observed in bulk electron doped $KTaO_3$, where no superconductivity has been observed (see Supplementary Fig. 2). Low temperature variation of R_S under $B_\perp$ has been shown in **d** (from 0 T to 0.1 T) and **e** (from 0.2 T to 9 T) for the Hall bar along [11$\bar{2}$]. Dotted lines in **e** show logarithmic dependence of R_S with the temperature near the avoided superconductor insulator transition.

obtained by tracking the evolution of superconducting transition, T_C with magnetic field from R_S vs. T plots. An appreciable difference in magnitude of $B_{C_\perp}$ is observed for two configurations of current. Higher value of $B_{C_\perp}$ for current along [11$\bar{2}$] direction is consistent with the observation of higher T_C for current along [11$\bar{2}$] direction. The solid line shows fitting with the Ginzburg-Landau (G-L) theory which predicts a linear T behavior of $B_{C_\perp}$ given by

$$B_{C_\perp} = \frac{\Phi_0(1 - T/T_C)}{2\pi(\xi_0)^2} \quad (1)$$

where Φ_0 is the magnetic flux quantum and ξ_0 is the G-L coherence length at $T = 0$ K. ξ_0 from fitting is found to be ~ 23.4 nm and 21.4 nm for current along [11$\bar{2}$] and [1$\bar{1}$0] directions, respectively. Figure 2b shows the temperature evolution of $B_{C_\parallel}$ for the case when current is parallel to the in plane magnetic field (see Supplementary Figs. 4–6 for R_S vs. T plots and data for other configurations of current). Similar to the out of plane measurement, the magnitude of $B_{C_\parallel}$ is found to be larger for the current along [11$\bar{2}$] direction. The temperature dependence of $B_{C_\parallel}$ shows a characteristic square-root dependence (shown by the solid lines in Fig. 2b). Such a behavior is consistent with the Tinkham's model[52] where $B_{C_\parallel}$ is given by

$$B_{C_\parallel} = \frac{\Phi_0[12(1 - T/T_C)]^{1/2}}{2\pi d\xi_0} \quad (2)$$

where d is the effective thickness of the superconducting region. The estimated thickness of superconducting region is found to be ~5 nm which is much less than phase coherence length, signifying two dimensional nature of the superconductivity at the AlO_x/KTO (111) interface. Interestingly, the value of the in plane upper critical field extrapolated to 0 K is found to be much larger (~10 T) than Clogston Chandrasekhar limit[53,54]. Such a large value of $B_{C_\parallel}$ is generally expected in systems with a strong SOC[55] and the observation of weak antilocalization characteristics in longitudinal magnetoconductance data within the normal phase (see Fig. 2c) demonstrates the importance of SOC in the present case.

In order to examine the extent of disorder in our system, we have estimated the ratio of ξ_0 and the electronic mean free path l_{mfp}. The ratio is close to 2, emphasizing that the SC at AlO_x/KTO (111) interface falls in the intermediate disorder regime (see Fig. 2d), making it an interesting system for simultaneous investigation of dissipation pertaining to an ideal BKT system and also arising from the inhomogeneous electronic structure using a single sample[56]. The presence of oxygen vacancies at the interface are one of the most

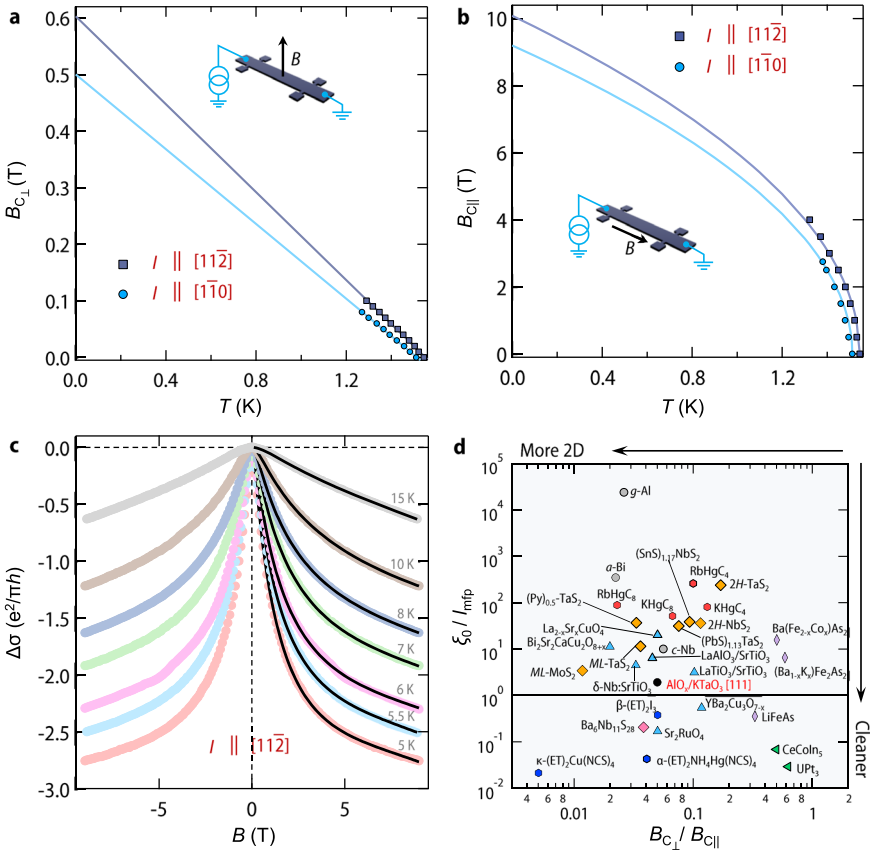

Fig. 2 Critical field, weak antilocalization, and the extent of disorder. a Temperature dependence of out of plane upper critical field ($B_{C_\perp}$) for I along [11$\bar{2}$] and [1$\bar{1}$0]. The solid line denotes fitting with Ginzburg-Landau theory. **b** Temperature dependence of in-plane upper critical field ($B_{C_\parallel}$) for I along [11$\bar{2}$] and [1$\bar{1}$0]. Further, B is parallel to the current direction. The solid line denotes fitting with Tinkham's model. **c**. Sheet conductance difference ($\Delta\sigma = \sigma(B) - \sigma(B=0)$, $\sigma = 1/R_S$ (B)) in the units of $e^2/\pi h$ for the Hall bar with I along [11$\bar{2}$]. The black solid curves show the fitting with ILP (Iordanskii, Lyanda-Geller, and Pikus) theory[70,71] (without considering linear Rashba term) including a classical B^2 term (also see Supplementary Note 2 and Supplementary Fig. 7 for fitting details). **d**. Phase diagram of several superconducting compounds categorized by their extent of 2D character and cleanliness. 2D character is resembled by the anisotropy of critical field defined by ($B_{C_\perp}/B_{C_\parallel}$) and extent of disorder is quantified by the ratio between phase coherence length and electronic mean free path (ξ_0/l_{mfp}). Assuming a single isotropic band in 2D, l_{mfp} is given by $l_{mfp} = h/(e^2 k_F R_S)$, where $k_F = (2\pi n_s)^{1/2}$ is the Fermi wave vector and n_s is the sheet carrier density. From the measured n_s (at 5 K) and R_S (at 5 K), the l_{mfp} is estimated to be ~12 nm for the present case. The value of all the parameters for other compounds have been largely taken from the reference[56] except for the $LaTiO_3/SrTiO_3$ interface which has been taken from reference[37]. As evident, $AlO_x/KTaO_3$ (111) is located very near to the boundary between clean and dirty limits, denoted by a horizontal solid line.

prominent sources of disorder in the system. Clustering of oxygen vacancies can also lead to a very local inhomogeneous electronic structure in the real space[57]. Apart from such local inhomogeneities, there is another source of inhomogeneity, which happens at a much larger scale, known as electronic phase separation (EPS)[29–32]. EPS has been routinely observed in STO based 2DEGs and is very often associated with the presence of multi carriers at the interface. The observation of two types of electrons with densities n_1 and n_2 with mobility μ_1, and μ_2, respectively ($n_1 >> n_2$ and $\mu_1 < \mu_2$) in our Hall effect measurements (see Supplementary Notes 3–5 and accompanying Supplementary Figs. 8–10) strongly suggests that a similar scenario can also be applicable in our samples. As a general consequence of EPS, superconducting puddles joined by weak links would emerge naturally in real space[38], making the SC strongly inhomogeneous. This mechanism is likely a dominant cause for the observed granular nature of our system. Note that EPS could also arise due to the Rashba SOC[29], which is also quite generic to our system.

Various regions of dissipations as a function of *dc* current. Having established the nature of inhomogeneities in our 2D superconducting system, we now explore the nature of dissipation under *dc* current bias. For this, comprehensive I-V measurements have been performed. Figure 3a shows the I–V curves taken in forward and backward sweeps at several fixed temperatures from 1.26 K to 10 K for current along [11$\bar{2}$] direction under zero magnetic field. All data has been shifted vertically upwards for visual clarity. Broadly four distinct regimes can be identified in the I–V curve at the lowest temperature (1.26 K) of our measurements: (1) at small currents (<60 μA—70 μA) while voltage drop looks almost independent of I, a small voltage drop always appears (see Fig. 3b)) due to breaking of few weakly bound vortex-antivortex pairs as the critical current for breaking of vortex-antivortex is zero[12,58]. (2) Above this regime, a non-linear behavior appears in a very short window from ~ 80 μA–110 μA. (3) This regime then translates into a region from 110 μA to 175 μA, where the majority of the dissipation happens as observed by a large change in the voltage drop. (4) Above 175 μA, the magnitude of V grows almost in proportion to the applied current and finally enters into the regime of ohmic dissipation. All these different regions in I-V characteristics are strongly T dependent. The first and fourth regimes are well understood[1,12] and are skipped from further discussions.

We first discuss the origin of non-linear I–V, observed just above the 1st regime. This regime corresponds to the intrinsic

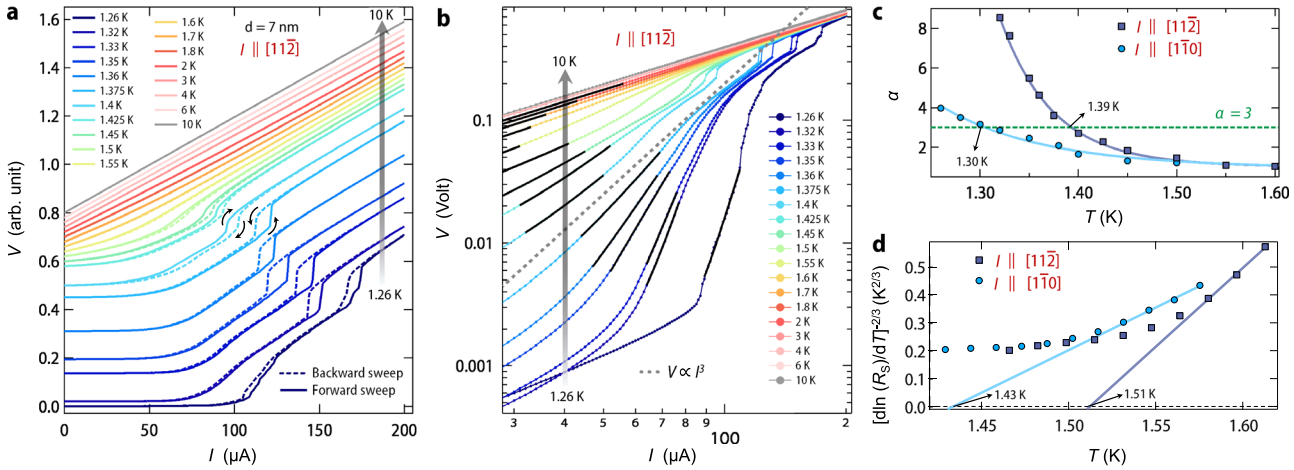

Fig. 3 Current-voltage (*I*–*V*) characteristics and determination of T_{BKT}. a Temperature dependent *I*–*V* curves measured in current bias mode for the Hall bar along [11$\bar{2}$]. Solid and dotted curves denote forward and backward sweeps, respectively. Curves have been shifted upward for visual clarity. **b** *I*–*V* curves in logarithmic scale during the forward sweep. The solid black line shows the fit with the power law given by $V \propto I^{\alpha}$. A dotted gray line corresponds to $\alpha = 3$ where the Berezinskii Kosterlitz Thouless transition takes place. **c** Temperature dependence of α for *I* along [11$\bar{2}$] and [1$\bar{1}$0]. A dotted green line shows a constant line for $\alpha = 3$. From the crossover of α around 3, T_{BKT} is found out to be 1.39 K and 1.30 K for the Hall bar along [11$\bar{2}$] and [1$\bar{1}$0], respectively **d**. The value of T_{BKT} is also estimated using the Halperin-Nelson model ($R_S = R_0 \exp[-b/(T-T_{BKT})^{1/2}]$ where *b* is the vortex-antivortex interaction strength)[63,72]. To estimate T_{BKT} using this model, $d\ln(R_S)/dT]^{-2/3}$ has been plotted as a function of *T*, near the superconducting transition temperature. By finding the *x* axis intercept of this plot, we find T_{BKT} ~1.51 K and 1.43 K for the Hall bar along [11$\bar{2}$] and [1$\bar{1}$0], respectively. These values are very close to the T_{BKT}, obtained in **c**.

dissipation of a BKT system, which is characterized by power law behavior ($V \propto I^{\alpha}$) arising from current driven unbinding of thermally generated vortex-antivortex pairs near the BKT transition[9,10]. This behavior becomes much more evident in the logarithmic plot (Fig. 3b), where power law translates into a linear behavior. The value of α becomes exactly 3 at the T_{BKT} (shown by a dotted gray line ($V \propto I^3$) in Fig. 3b) and is routinely used to trace out BKT phase transition in 2D superconductors. T_{BKT} is estimated to be 1.39 K and 1.30 K (Fig. 3c) for the Hall bar along [11$\bar{2}$] and [1$\bar{1}$0], respectively, from such analysis (also see Fig. 3d).

Demonstration of LO-type FFI. We next focus on the nature of dissipation beyond power-law regime. At the lowest temperature of our measurement 1.26 K, which is below T_{BKT}, dissipation happens via discrete jumps in the measured voltage, which is much more evident from the *dV*/*dI* plot shown in Supplementary Fig. 11. These are reminiscent of phase slip events generally observed in 1D superconducting wire[1]. On the contrary, formation of hot-spots[59] and flux-flow instability[18,21] are the two widely accepted cause for such discrete jumps under large current in thin film geometry. Hot-spots are the regions in real space with temperature higher than the T_C, which appear due to the Joule self-heating in inhomogeneous systems[60]. In presence of hot-spots, *I*–*V* curve takes the shape of '*S*', which would lead to a hysteresis between forward and reverse current bias (see Fig. 4a). In the present case, hot-spots are most likely to occur near the weak links joining the superconducting puddles, appearing due to the granular nature of SC as discussed earlier.

Apart from the hot-spot effect, LO type FFI is another phenomenon which leads to a 'S' shape *I*–*V* characteristics with similar voltage instabilities in current bias mode due to ultra-fast vortices[18,19]. While the original LO instability was predicted for type II superconductors under magnetic field, we demonstrate here that such unusual phenomenon can be observed in 2D superconductors, even in absence of a magnetic field. This is due to the fact that free vortices can be generated in 2D superconductors either by thermal fluctuation in the temperature range $T_{BKT} \le T \le T_C$[11,61] or by breaking of thermally induced vortex-antivortex pairs by current below T_{BKT}[10]. In the following, we test the applicability and predictions of LO theory for the AlO_x/KTO (111) superconductor. We further emphasize that the magnetic field generated due to current flowing through the sample or residual field in the magnet is too small and has no role for our observation (see Supplementary Notes 6 and 7 and accompanying Supplementary Figs. 12 and 13).

1. The whole LO theory of FFI was built on the argument that at large vortex velocities, quasiparticles at the core of the vortex can reach energies above the superconducting energy gap (Δ) due to its acceleration under electric field created due to flux-flow and ultimately diffuse away from the core. During this process, the core of the vortex starts shrinking and resultantly, the viscous damping coefficient (η) becomes a function of vortex velocity which is given by the formula[18,19]

$$\eta(v) = \eta(0)\frac{1}{1+(v/v^*)^2} \quad (3)$$

where v^* is the critical vortex velocity, where FFI would occur. As evident from the above equation, η decreases with increasing *v*, leading to an ever increasing vortex velocity and after the critical velocity v^*, the system becomes unstable, leading to a voltage jump in *I*-*V* curve.
In order to check this, we have calculated the vortex velocity (see Supplementary Note 8) using the Gor'kov-Josephson relation[62,63]. Figure 4b shows the calculated velocity for 7 nm AlO_x/KTO (111) sample at 1.26 K in zero magnetic field. As evident, there is almost two orders of magnitude abrupt increase in the vortex velocity (see Fig. 4b), consistent with the LO-type FFI. Moreover, the maximum velocity (~10^5 ms^{-1}) is much higher than the Abrikosov vortex velocity (~10^3 ms^{-1})[1], and is also very similar to what has been reported earlier for other systems exhibiting LO-type instability under magnetic field[27].
2. In the original LO picture, the sample is assumed to be in perfect thermal equilibrium with the phonon bath and

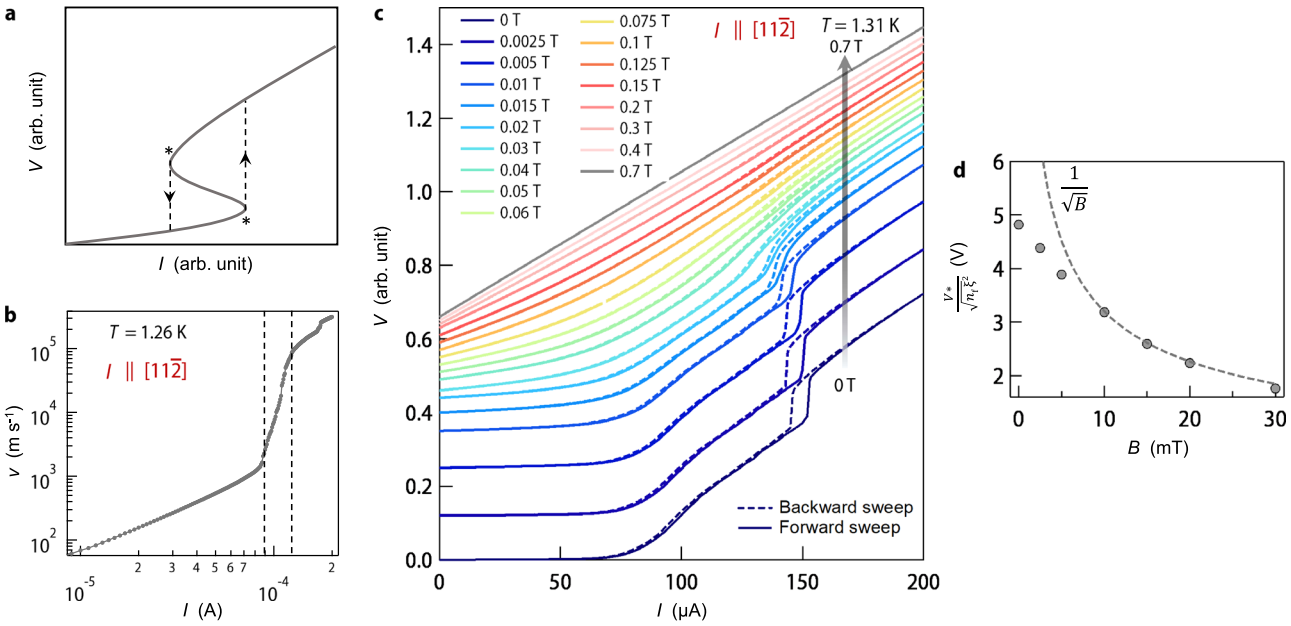

Fig. 4 Evidence for flux-flow instability. a A schematic depicting 'S' shaped *I*–*V* characteristics. which has two unstable points, denoted by asterisk symbol. When the *I*–*V* measurement is performed in current bias mode, a voltage instability is observed when the value of current is close to unstable point leading to an abrupt increase/decrease in the voltage drop. Further, the voltage instability under backward current sweep happens at a lower current than in the forward sweep leading to a hysteresis. **b** Current dependent vortex velocity at 1.26 K for 7 nm $AlO_x/KTaO_3$ (111) (*I* along [11$\bar{2}$]). We emphasize that this whole analysis only holds only in between the region marked with the dashed lines[28]. **c** Magnetic field dependent *I*–*V* curves measured in current bias mode for the Hall bar along [11$\bar{2}$] on 7 nm $AlO_x/KTaO_3$ (111) sample at 1.31 K. Curves have been shifted upward for visual clarity. **d** Magnetic field evolution of normalized critical voltage ($\frac{V^*}{\sqrt{n_f\xi^2}}$) calculated for Hall bar along [11$\bar{2}$] on 7 nm $AlO_x/KTaO_3$ (111) sample. The dotted line denotes expected behavior for $1/\sqrt{B}$ *dependence*.

hence the effect of Joule heating on FFI is completely neglected. However, this may not be true in reality. In presence of overheating, a further modification has been suggested by Bezuglyj and Shklovskij[27,64], which would lead to a B dependent v^* with functional form

$$v^* \propto z\Delta^{1/2}B^{-1/2} \tag{4}$$

where z is the heat removal coefficient. However, this relation was derived with the constraint that density of free vortices (n_f) is independent of temperature, which is not the case in 2D superconductors. For BKT system, the expression for v^* in presence of overheating can be written as (see Supplementary Note 9)

$$v^* \propto \left(\frac{\Delta(T)\xi^2(T)}{n_f(T,B)}\right)^{1/2} B^{-1/2} \tag{5}$$

Since the exact temperature dependence of ξ is unknown, we rewrite the above equation using the Gor'kov-Josephson relation[62,63] as

$$\frac{V^*}{\sqrt{n_f\xi^2}} \propto \Delta(T)^{1/2}B^{-1/2} \tag{6}$$

where V^* marks the onset of voltage instability in *I*–*V* curve.

To testify this for present case, we have performed *I*–*V* measurement in presence of B at a fixed temperature. Figure 4c shows one representative set of data for Hall bar along [11$\bar{2}$] on 7nm AlO_x/KTO (111) sample. As evident from Fig. 4d, normalized V^* is indeed dependent on B with a characteristic of $B^{-1/2}$ dependence at higher fields (for calculation of the denominator in Eq. (6), we refer to Supplementary Note 10). We note that, a similar behavior was observed for v^* in Nb-C superconductor near T_C and the deviation from $B^{-1/2}$ at low fields was attributed to the possible role of edge controlled FFI[27].

Discussions

Having demonstrated the relevance of hot-spots and LO type FFI in our samples, we next discuss the temperature evolution of these two effects. For this, we first note that since the specific heat transfer power from the sample to the thermal bath is not known at a given temperature, a quantitative estimation of relative contribution from the hot-spot and FFI can not be made. Nonetheless, our temperature-dependent analysis of $\frac{V^*}{\sqrt{n_f\xi^2}}$ indicates that the hot-spots are most likely effective below T_{BKT} whereas FFI would be more applicable close to T_C (see Supplementary Note 11 and Supplementary Fig. 14).

We next focus on the temperature evolution of the *I*-*V* hysteresis [Fig. 3a] in our samples. The hysteresis is anticlockwise at the lowest temperature of our measurement, which can be attributed jointly to the formation of hot-spots and FFI as discussed earlier. Surprisingly, the nature of hysteresis changes completely from anticlockwise to clockwise above a certain temperature (highlighted by arrows in Fig. 3a). We have also observed the same behavior for another sample with 14 nm AlO_x thickness (see Supplementary Figs. 16–18 for additional data on this sample). Such clockwise hysteresis is extremely rare[21] and has never been observed in any interfacial superconductors to the best of our knowledge. To visualize this drastic change in *I*-*V* hysteresis, we further plot the maximum width of hysteresis (δI_c) as a function of temperature. Figure 5a corresponds to δI_c for Hall bar along [11$\bar{2}$] and [1$\bar{1}$0] directions (also see Supplementary Fig. 15) on 7 nm AlO_x/KTO (111) sample. Figure 5b contains a similar set of data for the 14 nm AlO_x/KTO (111) sample. As clearly evident, hysteresis always changes its sign around the T_{BKT} and vanishes around T_C in all the four Hall bars, that we have investigated in

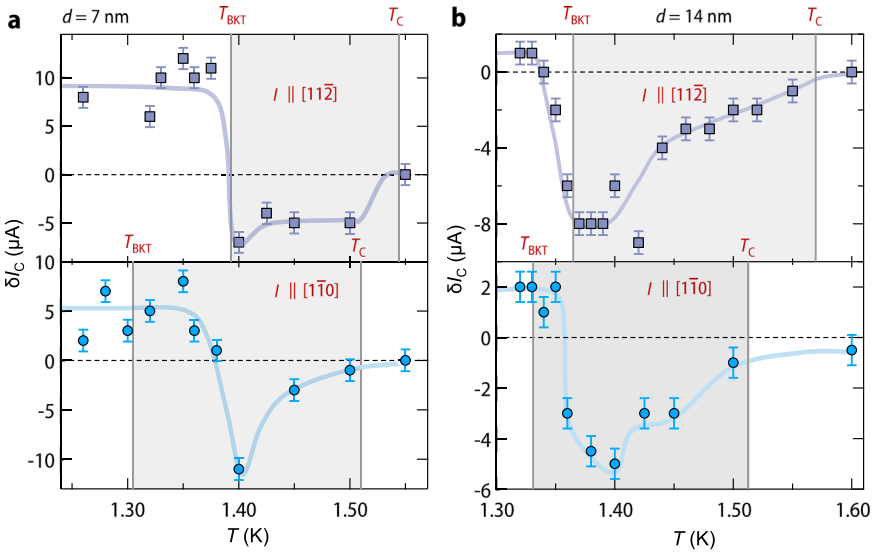

Fig. 5 Sign change of hysteresis across Berezinskii Kosterlitz Thouless transition. a Maximum width of hysteresis [$\delta I_c = (I_c)_{forward}$-$(I_c)_{backward}$, $(I_c)_{forward}$, and $(I_c)_{backward}$ are the values of critical current in the middle of hysteresis in the forward and backward sweep, respectively] for I along [11$\bar{2}$] and [1$\bar{1}$0] for 7 nm $AlO_x/KTaO_3$ (111) sample. **b** Similar data for another sample having 14 nmAlO_x. The sheet carrier density for this sample was found to be 1.1×10^{14} cm^{-2} at 300 K and the T_C is 1.57 K and 1.51 K for I along [11$\bar{2}$] and [1$\bar{1}$0] respectively. These values are very similar to the case of 7 nm $AlO_x/KTaO_3$ (111) sample. The change in the width of the hysteresis upon multiple cycling has been used to estimate the error bar.

this work. While the vanishing of anticlockwise hysteresis across T_{BKT} can be accounted by the disappearance of quasi 1D dissipating channels such as weak links[65], the clockwise hysteresis can not be explained by the hot-spot effect. Rather, the observation of clockwise hysteresis in I-V can be explained by (i) vortex de-pinning like instabilities[66] or (ii) LO type FFI[21]. Since our sample is already in flux-flow regime (see Supplementary Note 12 and Supplementary Fig. 19) at currents much smaller than the current at which the voltage instability is observed, the possibility of vortex de-pinning like instabilities can be discarded[24]. We further recall the following proposition of Samoilov et al. in the context of LO theory[21]. It was proposed that, once the superconductor is driven into the normal resistive state in the forward current sweep, the electron-electron (inelastic) scattering rate becomes higher (smaller τ_e)[21], leading to an electronic instability. This would mean that during the backward current sweep, the value of V^* will be higher ($V^* \sim \tau_e^{-1/2}$) than that of the forward sweep (see Supplementary Note 9). This would automatically move the I–V curve towards the higher current and would result to a clockwise hysteresis, as observed here. Moreover, the vanishing of clockwise hysteresis at T_C is consistent with the fact that vortices do not exist above T_C.

Conclusions

In summary, our extensive analysis of temperature and magnetic field dependent I-V measurement strongly emphasizes on the definite role of heating effects and FFI in determining the nature of dissipation at large current bias in inhomogeneous BKT systems. The in-plane anisotropy observed in the onset temperature of clockwise hysteresis between the two Hall bars with I along [1$\bar{1}$0] and [11$\bar{2}$] may arise from the in-plane anisotropy of critical vortex velocity for the onset of electronic instability. Such an observation is beyond the LO theory and calls for further investigations. Since the vortex structure in BKT system is strongly influenced by the presence of strong SOC[67], an extension of LO theory in presence of SOC and finite heating effects will be essential to understand such non-trivial feature. Future studies will focus on measurements beyond the intermediate disorder regime under simultaneous top and bottom gate, which will provide an independent investigation of the role of disorder and carrier density in determining the nature of dissipation under large current drive. Several recent studies, including those focused on magic angle twisted bilayer graphene[68], MoS_2[28], and $NbSe_2$[16], have observed anomalies in high-current I–V characteristics, which have been explained qualitatively in terms of vortex instability/phase-slip lines. Our findings of FFI across the BKT phase transition could serve as a framework for comprehending dissipation in such diverse class of 2D superconductors subjected to large currents. Further exploration of this highly non-equilibrium phenomenon in other systems that exhibit BKT transition, such as trapped atomic gases and neutral superfluids, would be of significant interest.

Methods

Sample growth and characterization. $AlO_x/KTaO_3$ (111) samples were fabricated by ablating a single crystalline Al_2O_3 target on (111) oriented KTO substrate using a pulsed laser deposition system (Neocera LLC, USA) equipped with a high pressure reflection high energy electron diffraction setup (Staib instruments, Germany). A KrF excimer laser (Coherent, Germany) operated at a repetition rate of 1 Hz ($\lambda = 248$ nm) and an energy density ~1 Jcm^{-2} (on the target) was used for ablating the target. Target to substrate distance was fixed at 5.6 cm. The substrate was heated using a resistive heater whose temperature was maintained at 560 °C during the growth. The growth chamber pressure was 5×10^{-6} Torr during the deposition. Immediately after the ablation, the sample was cooled to room temperature at a rate of 15°Cmin^{-1} under the vacuum. The surface morphology of the as received substrate and the film was monitored by performing atomic force microscopy (AFM) in non-contact mode using a Park AFM system. The thickness of the films was determined from X-ray reflectivity measurement performed in a lab based Rigaku Smartlab diffractometer. For more details, see Supplementary Note 1.

Transport measurements. All the transport measurements were performed in an Oxford Integra LLD system using the standard four probe method in the Hall bar geometry. Ohmic contacts were made by ultrasonically bonding Al wire. Electrical resistance was measured using a *dc* delta mode with a Keithley 6221 current source and a Keithley 2182A nanovoltmeter and also using standard low-frequency lock-in technique. For I–V measurements, a Keithley 2450 source meter was used in current bias mode with a sweep rate of 10 μAs^{-1}.

Data availability

The data that support the findings of this work are available from the corresponding authors upon reasonable request.

Received: 17 April 2023; Accepted: 23 May 2023;
Published online: 05 June 2023

References

1. Tinkham, M. *Introduction to superconductivity* (Courier Corporation, 2004).
2. Bardeen, J. Critical fields and currents in superconductors. *Rev. Mod. Phys.* **34**, 667–681 (1962).
3. Embon, L. et al. Imaging of super-fast dynamics and flow instabilities of superconducting vortices. *Nat. Commun.* **8**, 85 (2017).
4. Devoret, M. H. & Schoelkopf, R. J. Superconducting circuits for quantum information: an outlook. *Science* **339**, 1169–1174 (2013).
5. Gurevich, A. & Ciovati, G. Dynamics of vortex penetration, jumpwise instabilities, and nonlinear surface resistance of type-ii superconductors in strong rf fields. *Phys. Rev. B* **77**, 104501 (2008).
6. Welp, U., Kadowaki, K. & Kleiner, R. Superconducting emitters of thz radiation. *Nat. Photon.* **7**, 702–710 (2013).
7. Berezinskii, V. Destruction of long-range order in one-dimensional and two-dimensional systems having a continuous symmetry group i. classical systems. *Sov. Phys. JETP* **32**, 493–500 (1971).
8. Kosterlitz, J. M. & Thouless, D. J. Ordering, metastability and phase transitions in two-dimensional systems. *J. Phys. C: Solid State Phys.* **6**, 1181–1203 (1973).
9. Beasley, M. R., Mooij, J. E. & Orlando, T. P. Possibility of vortex-antivortex pair dissociation in two-dimensional superconductors. *Phys. Rev. Lett.* **42**, 1165–1168 (1979).
10. Epstein, K., Goldman, A. M. & Kadin, A. M. Vortex-antivortex pair dissociation in two-dimensional superconductors. *Phys. Rev. Lett.* **47**, 534–537 (1981).
11. Resnick, D. J., Garland, J. C., Boyd, J. T., Shoemaker, S. & Newrock, R. S. Kosterlitz-thouless transition in proximity-coupled superconducting arrays. *Phys. Rev. Lett.* **47**, 1542–1545 (1981).
12. Jos, J. V.*40 Years of Berezinskii-Kosterlitz-Thouless Theory* (World Scientific, 2013).
13. Andronov, A., Gordion, I., Kurin, V., Nefedov, I. & Shereshevsky, I. Kinematic vortices and phase slip lines in the dynamics of the resistive state of narrow superconductive thin film channels. *Phys. C Supercond. Appl.* **213**, 193–199 (1993).
14. Weber, A. & Kramer, L. Dissipative states in a current-carrying superconducting film. *J. Low Temp. Phys.* **84**, 289–299 (1991).
15. Sivakov, A. G. et al. Josephson behavior of phase-slip lines in wide superconducting strips. *Phys. Rev. Lett.* **91**, 267001 (2003).
16. Paradiso, N., Nguyen, A.-T., Enzo Kloss, K. & Strunk, C. Phase slip lines in superconducting few-layer nbse2 crystals. *2D Materials* **6**, 025039 (2019).
17. Berdiyorov, G. R., Milošević, M. V. & Peeters, F. M. Kinematic vortex-antivortex lines in strongly driven superconducting stripes. *Phys. Rev. B* **79**, 184506 (2009).
18. Larkin, A. & Ovchinnikov, Y. Nonlinear conductivity of superconductors in the mixed state. *Sov. Phys. JETP* **41**, 960–965 (1975).
19. Klein, W., Huebener, R. P., Gauss, S. & Parisi, J. Nonlinearity in the flux-flow behavior of thin-film superconductors. *J. Low Temp. Phys.* **61**, 413–432 (1985).
20. Doettinger, S. G. et al. Electronic instability at high flux-flow velocities in high-T_c superconducting films. *Phys. Rev. Lett.* **73**, 1691–1694 (1994).
21. Samoilov, A., Konczykowski, M., Yeh, N.-C., Berry, S. & Tsuei, C. Electric-field-induced electronic instability in amorphous mo 3 si superconducting films. *Phys. Rev. Lett.* **75**, 4118 (1995).
22. Ruck, B. J., Abele, J. C., Trodahl, H. J., Brown, S. A. & Lynam, P. Vortex dynamics and instabilities in layered and homogeneous ta/ge superconductors. *Phys. Rev. Lett.* **78**, 3378–3381 (1997).
23. Xiao, Z. L., Andrei, E. Y. & Ziemann, P. Coexistence of the hot-spot effect and flux-flow instability in high-T_c superconducting films. *Phys. Rev. B* **58**, 11185–11188 (1998).
24. Xiao, Z. L., Voss-de Haan, P., Jakob, G. & Adrian, H. Voltage jumps in current-voltage characteristics of $bi_2sr_2cacu_2o_{8+\delta}$ superconducting films: Evidence for flux-flow instability under the influence of self-heating. *Phys. Rev. B* **57**, R736–R739 (1998).
25. Kunchur, M. N. Unstable flux flow due to heated electrons in superconducting films. *Phys. Rev. Lett.* **89**, 137005 (2002).
26. Babić, D., Bentner, J., Sürgers, C. & Strunk, C. Flux-flow instabilities in amorphous $nb_{0.7}ge_{0.3}$ microbridges. *Phys. Rev. B* **69**, 092510 (2004).
27. Dobrovolskiy, O. V. et al. Ultra-fast vortex motion in a direct-write nb-c superconductor. *Nat. Commun.* **11**, 3291 (2020).
28. Saito, Y., Itahashi, Y. M., Nojima, T. & Iwasa, Y. Dynamical vortex phase diagram of two-dimensional superconductivity in gated Mos_2. *Phys. Rev. Mater.* **4**, 074003 (2020).
29. Caprara, S., Peronaci, F. & Grilli, M. Intrinsic instability of electronic interfaces with strong rashba coupling. *Phys. Rev. Lett.* **109**, 196401 (2012).
30. Caprara, S. et al. Inhomogeneous multi carrier superconductivity at $laxo_3$/$srtio_3$(x = al or ti) oxide interfaces. *Supercond. Sci. Technol.* **28**, 014002 (2014).
31. Caprara, S. et al. Multiband superconductivity and nanoscale inhomogeneity at oxide interfaces. *Phys. Rev. B* **88**, 020504 (2013).
32. Ariando, X. et al. Electronic phase separation at the laalo3/srtio3 interface. *Nat. Commun.* **2**, 188 (2011).
33. Likharev, K. K. Superconducting weak links. *Rev. Mod. Phys.* **51**, 101–159 (1979).
34. Benyamini, A. et al. Fragility of the dissipationless state in clean two-dimensional superconductors. *Nat. Phys.* **15**, 947–953 (2019).
35. Reyren, N. et al. Superconducting interfaces between insulating oxides. *Science* **317**, 1196–1199 (2007).
36. Kozuka, Y. et al. Two-dimensional normal-state quantum oscillations in a superconducting heterostructure. *Nature* **462**, 487–490 (2009).
37. Biscaras, J. et al. Two-dimensional superconductivity at a mott insulator/band insulator interface latio3/srtio3. *Nat. Commun.* **1**, 89 (2010).
38. Chen, Z. et al. Carrier density and disorder tuned superconductor-metal transition in a two-dimensional electron system. *Nat. Commun.* **9**, 4008 (2018).
39. Changjiang, L. et al. Two-dimensional superconductivity and anisotropic transport at ktao3 (111) interfaces. *Science* **371**, 716–721 (2021).
40. Zheng, C. et al. Electric field control of superconductivity at the laalo3/ktao3(111) interface. *Science* **372**, 721–724 (2021).
41. Ren, T. et al. Two-dimensional superconductivity at the surfaces of $ktao_3$ gated with ionic liquid. *Sci. Adv.* **8**, eabn4273 (2022).
42. Mallik, S. et al. Superfluid stiffness of a ktao3-based two-dimensional electron gas. *Nat. Commun.* **13**, 4625 (2022).
43. Pai, Y.-Y., Tylan-Tyler, A., Irvin, P. & Levy, J. Physics of srtio3-based heterostructures and nanostructures: a review. *Rep. Prog. Phys.* **81**, 036503 (2018).
44. Liu, C. et al. Tunable superconductivity and its origin at ktao3 interfaces. *Nat. Commun.* **14**, 951 (2023).
45. Cui-Zu, C. et al. Experimental observation of the quantum alous hall effect in a magnetic topological insulator. *Science* **340**, 167–170 (2013).
46. Ojha, S. K. et al. Electron trapping and detrapping in an oxide two-dimensional electron gas: The role of ferroelastic twin walls. *Phys. Rev. Appl.* **15**, 054008 (2021).
47. Goldman, A. M. & Marković, N. Superconductor-insulator transitions in the two-dimensional limit. *Phys. Today* **51**, 39–44 (1998).
48. Haviland, D. B., Liu, Y. & Goldman, A. M. Onset of superconductivity in the two-dimensional limit. *Phys. Rev. Lett.* **62**, 2180–2183 (1989).
49. Kapitulnik, A., Kivelson, S. A. & Spivak, B. Colloquium: anomalous metals: failed superconductors. *Rev. Mod. Phys.* **91**, 011002 (2019).
50. Beloborodov, I. S., Lopatin, A. V., Vinokur, V. M. & Efetov, K. B. Granular electronic systems. *Rev. Mod. Phys.* **79**, 469–518 (2007).
51. Zhang, X., Hen, B., Palevski, A. & Kapitulnik, A. Robust anomalous metallic states and vestiges of self-duality in two-dimensional granular in-inox composites. *npj Quant. Mater.* **6**, 30 (2021).
52. Tinkham, M. Effect of fluxoid quantization on transitions of superconducting films. *Phys. Rev.* **129**, 2413–2422 (1963).
53. Chandrasekhar, B. S. A note on the maximum critical field of high-field superconductors. *Appl. Phys. Lett.* **1**, 7–8 (1962).
54. Clogston, A. M. Upper limit for the critical field in hard superconductors. *Phys. Rev. Lett.* **9**, 266–267 (1962).
55. Werthamer, N. R., Helfand, E. & Hohenberg, P. C. Temperature and purity dependence of the superconducting critical field, H_{c2}. iii. electron spin and spin-orbit effects. *Phys. Rev.* **147**, 295–302 (1966).
56. Devarakonda, A. et al. Clean 2d superconductivity in a bulk van der waals superlattice. *Science* **370**, 231–236 (2020).
57. Ojha, S. K. et al. Oxygen vacancy induced electronic structure modification of $ktao_3$. *Phys. Rev. B* **103**, 085120 (2021).
58. Kadin, A. M., Epstein, K. & Goldman, A. M. Renormalization and the kosterlitz-thouless transition in a two-dimensional superconductor. *Phys. Rev. B* **27**, 6691–6702 (1983).
59. Gurevich, A. V. & Mints, R. G. Self-heating in normal metals and superconductors. *Rev. Mod. Phys.* **59**, 941–999 (1987).
60. Skocpol, W. J., Beasley, M. R. & Tinkham, M. Self-heating hotspots in superconducting thin-film microbridges. *J. Appl. Phys.* **45**, 4054–4066 (1974).
61. Doniach, S. & Huberman, B. A. Topological excitations in two-dimensional superconductors. *Phys. Rev. Lett.* **42**, 1169–1172 (1979).
62. Josephson, B. D. Supercurrents through barriers. *Adv. Phys.* **14**, 419–451 (1965).
63. Halperin, B. I. & Nelson, D. R. Resistive transition in superconducting films. *J. Low Temp. Phys.* **36**, 599–616 (1979).
64. Bezuglyj, A. I. & Shklovskij, V. A. Effect of self-heating on flux flow instability in a superconductor near tc. *Phys. C Supercond.* **202**, 234–242 (1992).

65. Ovadyahu, Z. Transition to zero vorticity in a two-dimensional superconductor. *Phys. Rev. Lett.* **45**, 375–378 (1980).
66. Liu, Y. et al. History effect in inhomogeneous superconductors. *Phys. Rev. B* **66**, 144510 (2002).
67. Devreese, J. P. A., Tempere, J. & Sá de Melo, C. A. R. Effects of spin-orbit coupling on the berezinskii-kosterlitz-thouless transition and the vortex-antivortex structure in two-dimensional fermi gases. *Phys. Rev. Lett.* **113**, 165304 (2014).
68. Cao, Y., Park, J. M., Watanabe, K., Taniguchi, T. & Jarillo-Herrero, P. Pauli-limit violation and re-entrant superconductivity in moiré graphene. *Nature* **595**, 526–531 (2021).
69. Xiao, D., Zhu, W., Ran, Y., Nagaosa, N. & Okamoto, S. Interface engineering of quantum hall effects in digital transition metal oxide heterostructures. *Nat. Commun.* **2**, 596 (2011).
70. Iordanskii, S., Lyanda-Geller, Y. B. & Pikus, G. Weak localization in quantum wells with spin-orbit interaction. *ZhETF Pisma Redaktsiiu* **60**, 199 (1994).
71. Ojha, S. K. et al. Oxygen vacancy-induced topological hall effect in a nonmagnetic band insulator. *Adv. Quant. Technol.* **3**, 2000021 (2020).
72. Minnhagen, P. The two-dimensional coulomb gas, vortex unbinding, and superfluid-superconducting films. *Rev. Mod. Phys.* **59**, 1001–1066 (1987).

Acknowledgements

Authors are thankful to Prof. Jak Chakhalian, Prof. Sumilan Banerjee, Prof. Manish Jain, Prof. Vibhor Singh and Sanat Kumar Gogoi for fruitful discussions and valuable comments about the manuscript. SM acknowledges a Department of Science and Technology (DST) Nanomission grant (DST/NM/NS/2018/246), SERB, India (Early Career Research Award: ECR/2018/001512, I.R.H.P.A Grant No. IPA/2020/000034), MHRD, Government of India under STARS research funding (STARS/APR2019/PS/156/FS) for financial support. The authors acknowledge the AFM, XRD, and wire bonding facility at the Department of Physics, IISc Bangalore. We are also thankful to Ranjan Kumar Patel for proofreading.

Author contributions

S.M. conceived and supervised the experiments. S.K.O. and P.M. carried out all experiments and contributed to data analysis and interpretation. S.K. and J.M. contributed to the initial experiments. S.K.O., P.M., and S.M. wrote the paper. All authors discussed the results.

Competing interests

The authors declare no competing interests.

Additional information

Supplementary information The online version contains supplementary material available at https://doi.org/10.1038/s42005-023-01251-8.

Correspondence and requests for materials should be addressed to Shashank Kumar Ojha or Srimanta Middey.

Peer review information *Communications Physics* thanks the anonymous reviewers for their contribution to the peer review of this work.

Reprints and permission information is available at http://www.nature.com/reprints

Publisher's note Springer Nature remains neutral with regard to jurisdictional claims in published maps and institutional affiliations.